LA-UR-96-0615

CONF-9606175--1

Title: **Micromechanics of Spall and Damage in Tantalum**

Author(s): A.K. Zurek
W.R. Thissell
J.N. Johnson
D.L. Tonks
R. Hixson

esented at: 6th International Conference on Metal Forming and Journal of Materials Processing4

ubmitted to:

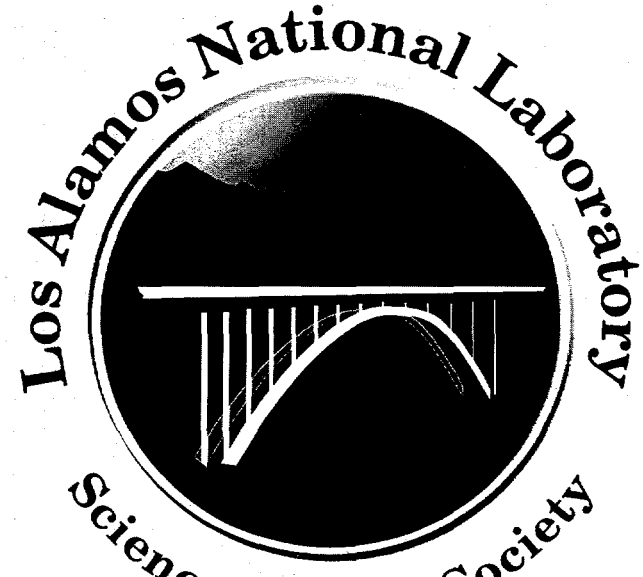

Los Alamos
National Laboratory

Micromechanics of Spall and Damage in Tantalum

Anna K. Zurek, W. Richards Thissell, James N. Johnson*, Davis L. Tonks**, and R. Hixson***
Materials Research and Processing Science
**Mechanics of Materials, ** Applied Theoretical Physics, ***Dynamic Experimentation*
Los Alamos National Laboratory
Los Alamos, NM 87545

Abstract

We conducted a series of plate impact experiments using an 80-mm launcher to study dynamic void initiation, linkup, and spall in tantalum. The tests ranged in peak shock pressures so that the effect of peak pressure on the transition from void initiation, incipient spall, and full spall could be studied. Wave profiles were measured using a velocity interferometry system (VISAR), and targets were recovered using "soft" recovery techniques. We utilized scanning electron microscopy, metallographic cross-sections, and plateau etching techniques to obtain quantitative information concerning damage evolution in tantalum under spall conditions. The data (wave profiles and micrographs) are analyzed in terms of a new theory and model of dynamic damage cluster growth.

1. Introduction

Spallation differs from other metal forming processes in several important respects. Stress waves travel during spallation at speeds great enough to form shock waves. This typically happens at very high strain rates. Typical high rate metal forming occurs at strain rates of 1-100 s^{-1}. Spallation occurs at strain rates of $> 10^5 s^{-1}$.

Spallation is one of a variety of experimental configurations that can produce controlled dynamic fracture for research purposes. Spallation is defined as a dynamic uniaxial strain fracture experiment. It occurs in a material due to tensile stresses generated by the interaction of two release (rarefaction) waves [1]. The principal stress components differ by the flow stress under conditions of dynamic uniaxial strain. Thus, in the ductile case, voids are subject to nearly isotropic tensile stress fields. Void growth and coalescence dominate all stages of the fracture process. Porosity, void formation, growth, and coalescence serve as variables in descriptions of spallation and therefore the fracture criteria of the material [1-3]. In a spallation plate impact experiment, an impactor is launched at a stationary plate sample. Impact results in loading that induces a shock wave at the impact plane. The shock waves travel from the impact plane to the flyer plate back surface and the target back surface. Reflection of the waves occur at the free surfaces. The two release shock waves meet inside the sample to produce a region of tension. The sample will fail within this region and separate into two pieces if the amplitude of the tensile wave exceeds the spall strength of the material. Otherwise, the sample will develop an incipient deformation zone within this region with characteristic voids, cracks, and plastic deformation.

The process of deformation and fracture can be investigated by using a "soft" sample recovery system and microscopic observations of the damage after the impact [1]. VISAR laser interferemetry can be employed to record the back free surface velocity of the target [4, 5]. Both techniques were utilized in this study of the spallation properties of high-purity tantalum subjected to a peak shock pressure just above the spallation threshold and to an impact stress one and one-half times the spallation threshold [6].

2. Material and Experiment Description

In this study we used commercially pure (triple electron beam arc melted) unalloyed tantalum plate with a measured composition of 6 ppm carbon, 24 ppm nitrogen, 56 ppm oxygen, < 1 ppm hydrogen, 19 ppm iron, 25 ppm nickel, 9 ppm chromium, 41 ppm tungsten, 26 ppm niobium, and the balance tantalum. The tantalum plate was in an annealed condition and had an equiaxed grain structure of 68 μm grain size [7]. We performed uniaxial strain spall tests utilizing an 80-mm single-stage launcher and recovery techniques as previously described [1]. VISAR interferemetry was used to record the free surface velocity of the samples [4, 5]. Tantalum samples were spalled at 9.5 and 17 GPa peak pressures and a 1 μs pulse duration under symmetric impact conditions. Recovered spalled samples were analyzed using optical and scanning electron microscopy to characterize the fracture morphology. The data (wave profiles and micrographs) were analyzed in terms of a new theory and model of dynamic damage cluster growth.

2.1. Spall Experiments

A number of previous reports have described shock compression and release in metals including tantalum [8-14]. Tantalum's mode of failure and hence, spall strength is known to be a function of shock amplitude. Previous recovery and non-recovery spall tests reported a 5.2 GPa spall strength for a 6 GPa

shock amplitude, 7.3 GPa spall strength for a 9.5 GPa shock amplitude, and 3.0 to 4.5 GPa spall strength for a 15 GPa shock amplitude [6, 7, 15]. These spall strength values compare favorably with our results. Figure 1 shows a typical calculated (using a void growth model without volumetric plasticity [2, 6]) and measured spall VISAR wave profile for high purity tantalum shock loaded to approximately 9.5 GPa. This calculated spall signal, assumes a simple tensile fracture model with a spall strength of 7.3 GPa. The peculiar observations associated with all 9.5 GPa spall VISAR signals is the sudden deceleration that occurs in the pull-back signal as shown in Figure 1.

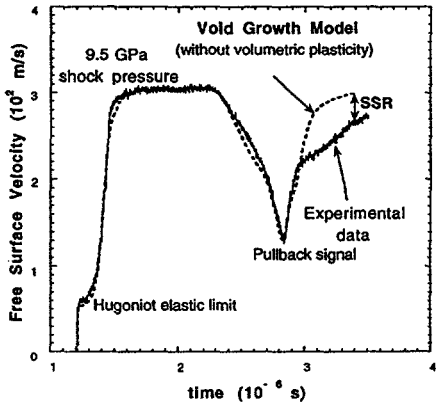

Figure 1. Void-growth model and spall VISAR trace at a shock pressure of 9.5 GPa.

The VISAR signal appearance of a sharp velocity pullback suggests that the material has undergone complete spallation, *i.e.*, physical separation into two pieces. However, there remains a restoring force to decelerate the spalled piece. This remained a puzzle until examination of a recovered spall sample disclosed the nature of the actual spall region. Figure 2 shows the spall region for the 9.5 GPa peak impact stress sample.

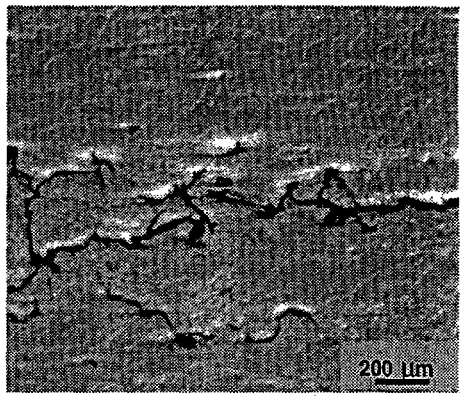

Figure 2. Spalled region for peak impact stress of 9.5 GPa.

Figure 2 shows that the spall region is not a distinct planar fracture surface, but it consists of a number of cracks extended over several hundred of microns in the direction of wave propagation (vertical

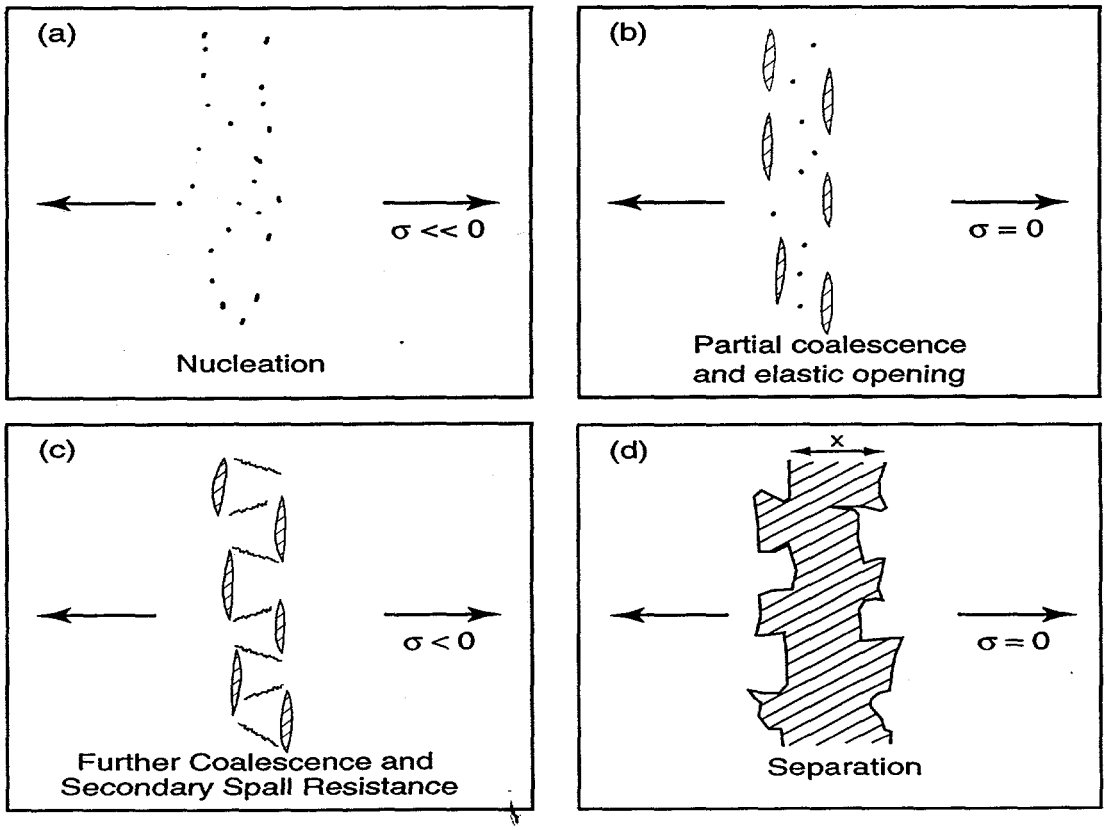

Figure 3. A heuristic picture of a proposed secondary spall mechanism.

on the micrograph). We suggest that the initial loss of material strength comes from the formation and elastic opening of cracks and hence, the corresponding drop of the longitudinal tensile stress. Following this initial loss of tensile strength, the extended spall region pulls apart and undergoes additional linking of these cracks to eventually form the separated spall fracture surface, but not before developing considerable secondary resistance to separation: this is what we refer to as secondary spall resistance (SSR).

Figure 3 shows a heuristic picture of the proposed secondary spall mechanism taking place in tantalum. Nucleation of voids takes place in the spall region when sufficient tensile stress is achieved ($\sigma<<0$, Figure 3a). Partial coalescence occurs in a preferential orientation following nucleation to relieve the longitudinal tensile stress component by the elastic opening of flat cracks parallel to the spall plane (Figure 3b). Further coalescence produces a "jig-saw-puzzle" effect that occurs in the next stage after the flat cracks have opened sufficiently (Figure 3c). This produces the observed secondary spall resistance. The spall region undergoes complete separation if the impact amplitude is high enough (Figure 3d). We believe that the pure tantalum sample shocked to a peak pressure of 9.5 GPa follows the spall process up to the point represented by Figure 3c, while the 17 GPa stress amplitude takes the sample to the point represented by Figure 3d *i. e.*, to complete separation.

The SSR is therefore included in the void growth model in terms of an additional tensile stress that develops following simple tensile fracture. As the separation distance x between the left and right sides of the spall surface increases, the SSR is given by:

$$\sigma_{SSR} = 0 \text{ for } x < a \text{ and } x > b \qquad (1)$$

$$\sigma_{SSR} = f\sigma_S[(x-b)/(b-a)] \text{ for } a<x<b \qquad (2)$$

where, σ_S is the absolute magnitude of the spall strength (here 7.3 GPa) and f is a dimensionless number less than unity. Generally a will be on the order of a few microns (the onset of SSR) and b will be on the order of a hundred microns (the end of SSR). Equations (1) and (2) represent the stress necessary to pull apart the convoluted spall region shown in Figure 3.

Calculations of the spallation behavior with the model including SSR is shown in Figure 4 for a = 5 microns, b = 200 microns, and f = 0.20, which fit very nicely the observed damage in the pure tantalum spall tests.

2.2. *Microscopy*

The spall test at a peak pressure of 9.5 GPa produced an incipient spall fracture. The cross section of the recovered spall sample showed distinctive cracks running across the entire diameter of the sample with multiple branched and interlocking cracks extending into the sample away from the principal fracture surface. The two halves of the spall sample did not separate from each other, regardless of the fact that

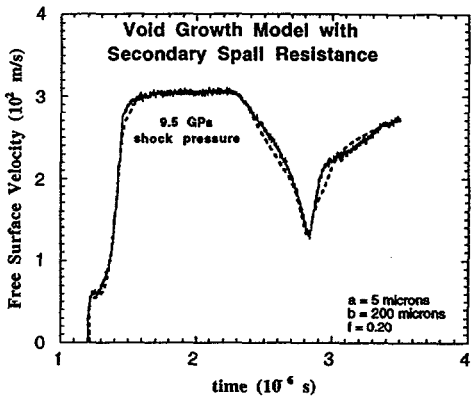

Figure 4. Void growth model with secondary spall resistance terms.

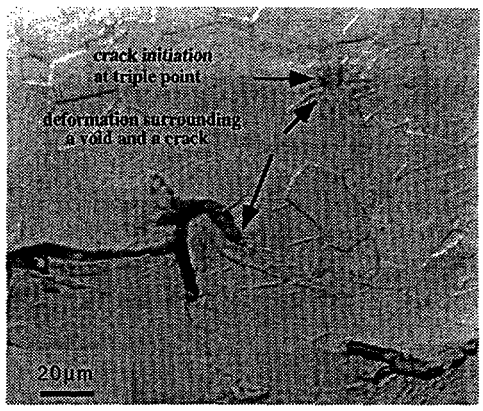

Figure 5. Cross section of tantalum sample spalled at 9.5 GPa showing void initiation at the point of intersection of several grains and propagating cracks with deformation surrounding a void and a crack (optical micrograph).

the peak pressure exceeded the expected spall strength of this material (see Figure 2).

Figure 5 shows a higher magnification view of the same spall cross section for the tantalum sample spalled at 9.5 GPa.

We sectioned off part of the spalled sample to allow the spall surfaces to separate. Figure 6 shows the typical ductile dimple fracture surface characteristic for metals in Group V_A tested at low strain rates and ambient temperatures. Multiple oxide or other impurities on the fracture surface are present, and most likely they are responsible for the void initiation.

The spall was complete and the two halves of the spalled sample fully separated to reveal fracture surface at a shock pressure of 17 GPa. Figure 7 is a micrograph of this sample and it shows a mixture of cleavage fracture and ductile dimples.

This change in the fracture morphology could be induced by significant deformation twinning occuring within the tantalum. Twin-twin interactions are known to be cleavage initiation sites [7]. The etched

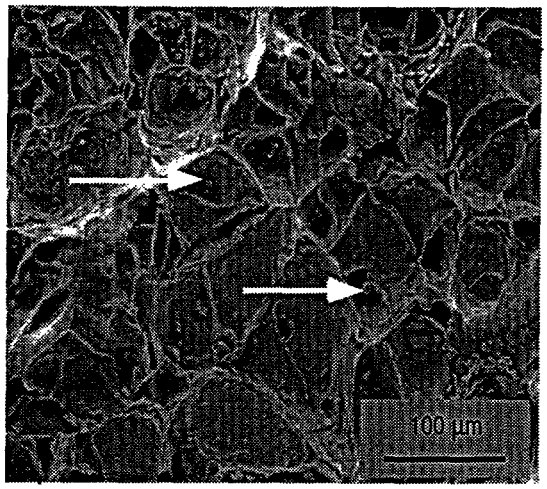

Figure 6. Spall fracture surface of tantalum spalled at 9.5 GPa. Arrows point to particles which most likely initiated dimples on the ductile fracture surface.

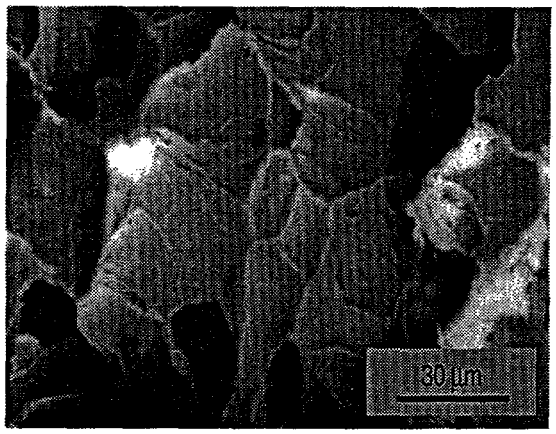

Figure 7. Fracture surface of tantalum spalled at 17 GPa peak pressure.

cross section, orthogonal to the spall fracture surface, revealed a significant density of deformation twins and only a few twins in the sample spalled at the lower peak pressure (Figure 5, Figure 8).

The sample tested at 17 GPa did not show crack branching, unlike the sample tested at 9.5 GPa. This observation, and the change in fracture mode from ductile to a mixture of ductile and cleavage fracture explains the observed decrease in spall strength with increased peak shock pressure in tantalum [6, 7, 15].

Cleavage fracture is associated with the ductile-to-brittle transition in this material especially under severe loading rates or low temperatures [7, 16]. High hydrostatic tensile stresses develop within the spall region. The ductile-to-brittle transition is pushed to higher temperatures with increases in the applied stress and hence, the applied strain rate. The fracture stress therefore increases because, to a first approximation, it is linearly proportional to the applied stress. The combination of this effect and a significant amount of deformation twinning initiates cleavage fracture.

Figure 8. Deformation twins present on the cross section of the tantalum sample spalled at 17 GPa.

2.3. A Micromechanical Model of Spall Events in Pure Tantalum

A theoretical program is underway to model the damage evolution observed in materials such as tantalum. A void-growth model with secondary spall resistance involves the mechanics of non-interacting spherical voids coupled with an ad hoc description of partial coalescence and elastic opening followed by crack link-up and finally, complete loss of strength [6]. On the other hand, a micromechanical model of spall is a theoretical analysis that attempts to explain, from more fundamental principles [17-20], the microscale interactions of voids to form the observed, complex fracture patterns (*e.g.*, Figures 2 and 5). Quantification of a micromechanical model, in combination with wave-propagation and spall calculations, should lead to an improved explanation of observed spall signals in materials undergoing void nucleation, growth and coalescence under dynamic loading conditions.

The micromechanical model includes damage induced by shear stress as well as damage caused by volumetric tension. Spallation is included in the model as a special case and strain induced damage is also treated. Void nucleation and growth are taken into account and give rise to strain rate effects, which also occur through elastic release wave propagation between damage centers (voids). The underlying physics of the model is the nucleation, growth, and coalescence of voids in a plastically flowing solid. The model is intended for hydrocode based computer simulation. The details of the model are published elsewhere [17-20], but a qualitative description of the model is presented below.

Voids are assumed to exist from time 0 of the deformation time in this micromechanical model, and they are randomly distributed throughout the material. A void may be an impurity, for example. Two voids coalesce when a local flow instability forms in the intervoid ligament, which then thins out during void growth. This process is called void linking. Each void is surrounded by a stress and strain linking range.

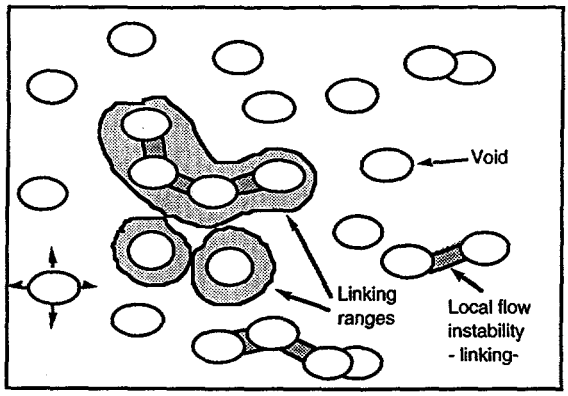

Figure 9. Statistical treatment of voids in a material.

Figure 9 represents the statistical consideration of the voids in any material. Arrows in the figure point to the voids, potential linking ranges (light gray) and local flow instabilities (dark gray).

The coalescence of two damage clusters (voids) requires the fulfillment of two conditions: sufficient stress and sufficient strain in the intervening ligament. An enhanced stress field around the periphery of large damage clusters leads to an enhanced stress link range. Material in the intervening ligament undergoes plastic flow under the applied external stress. The intervening ligament thins out when sufficient plastic flow accumulates. The degree of plastic flow necessary to thin out the ligament between two clusters is approximately inversely proportional with respect to the distance between them, because of the local unloading resulting in an elastic region surrounding damage clusters and neighboring voids. This results in the stress and strain concentration at the periphery of damage clusters and voids (Figure10).

Two modes of fracture can be represented that are functions of the rate of void growth and coalescence, which are in turn a function of the tensile peak amplitude, pulse duration, strain rate, and the sound velocity of the material.

The first mode of fracture, which we will refer to as a single crack fracture mechanism, is dominated by a stress linking enhancement which is an increasing function of the cluster size. The stress linking enhancement can occur at rates of void growth and coalescence lower than the second mode of fracture. A limiting condition for the occurrence of the stress linking enhancement is that the loading pulse duration exceeds the damage cluster diameter divided by the sound velocity of the material. This defines the time needed after initial loading for the establishment of the stress enhancement at the damage cluster periphery. The enhancement occurs *via* sound (release) wave propagation from one end of the damage cluster to the other end. Figure 10 illustrates the stress linking range, regions of instability, and the development of a rigid zone that form while a void is being linked into a growing damage cluster.

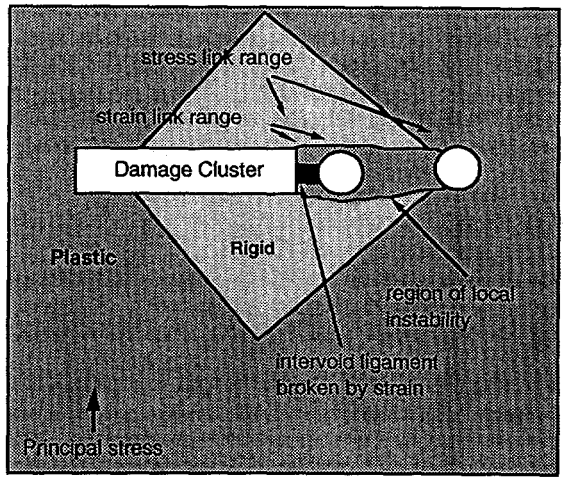

Figure 10. Single void linking to a damage cluster.

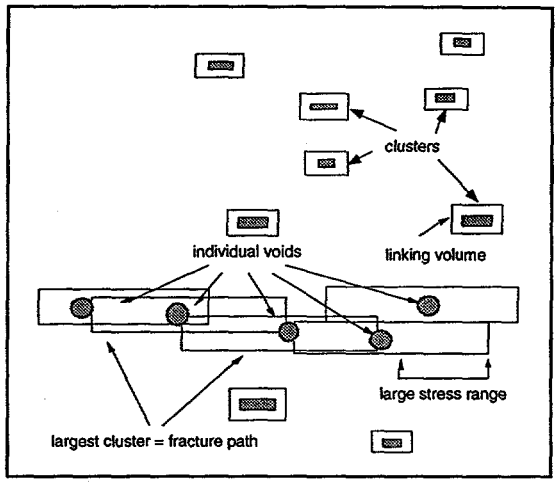

Figure 11. Single crack fracture mechanism.

This process is highly **deterministic**. Fracture will occur when the largest damage cluster grows much faster than small clusters *via* void coalescence. Figure 11 depicts this process. Due to the nature of this process, this will happen at the lower end of the high strain rate regime of dynamic deformation ($\dot{\varepsilon} \leq 10^5 s^{-1}$).

The stress linking enhancement is inhibited in the second mode of fracture, at higher rates of void growth and coalescence and when the pulse duration does not exceed the typical damage cluster diameter divided by the sound velocity. Failure occurs when the independently growing damage cluster linking ranges happen to overlap, forming a continuous fracture surface. This is a **stochastic** process similar to percolation, hence the name percolation fracture criteria which describes this process.

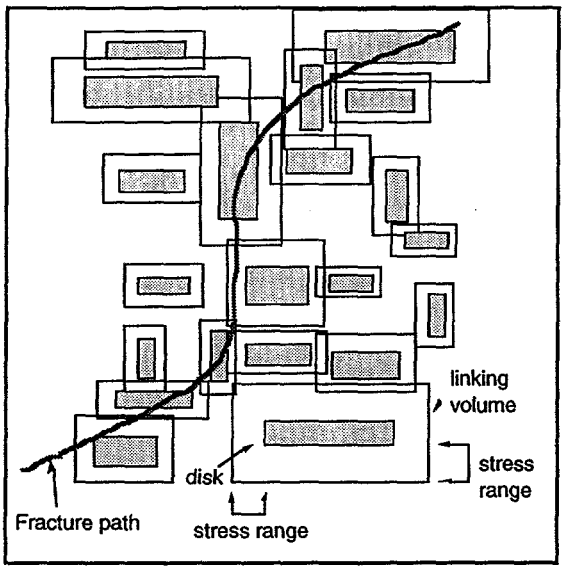

Figure 12. Percolation fracture criteria.

Figure 12 depicts this process and it is expected to happen at higher strain rates ($\dot{\varepsilon} \geq 10^5 s^{-1}$). The growth of large clusters is expected to be inhibited by the lack of time to form stress enhancements at a damage cluster (disk) periphery, and damage will form independently everywhere until it is connected into a continuous fracture path. The shallow dimple depth (Figure 6) of the spall plane and the small thickness of the crack nodes of the cross section micrographs (Figure 5, Figure 6) can be interpreted as small voids and failed intervoid ligaments. The plastic flow field surrounding a small void plausibly approximates the void link range (Figure 13). The void link range is very large due to the high spall strength of tantalum.

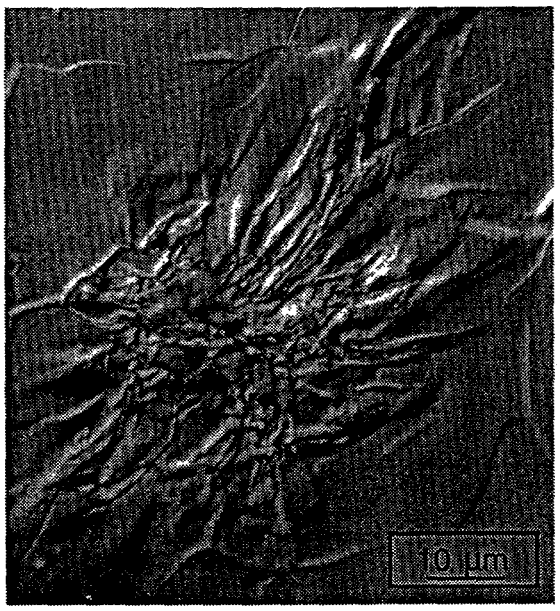

Figure 13. Etched cross section of a plastic field surrounding a void.

Computer calculations show that the loading time was too short for cluster peripherial stress enhancement to occur in this case [21]. These two occurrences support and favor the percolation process.

Qualitative correlations suggest that spall in high purity tantalum occurs by linking of widely separated voids *via* the percolation process.

3. Summary

Spall experiments on pure tantalum were performed over a range of shock peak pressures covering the transition from void initiation, incipient void linkup, to full fracture. These experiments have allowed the microstructural mechanisms of spallation to be studied and verified qualitatively. Shock pressures above the spall strength of the pure tantalum studied do not necessary lead to complete fracture. This is explained by a proposed model that incorporates a secondary spall resistance that follows the initial partial coalescence and elastic opening of voids. The secondary spall resistance is included in a proposed micromechanical model. The micromechanical model consists of two representations of fracture mechanisms that depend on the deformation strain rate. The mechanism that occurs at lower strain rates is called the single crack fracture mechanism. This mechanism arises due to an enhanced stress and strain fields around the periphery of large damage clusters. These fields interact in a highly deterministic process of void coalescence. The second fracture mechanism, the percolation fracture mechanism, occurs at higher strain rates where void growth occurs rapidly and independently throughout the fracture region. The process is stochastic and is reminiscent of percolation theory. A fracture surface is formed when the growing voids intersect by chance and form a continuous path.

This micromechanical explanation of dynamic fracture suggests that pure tantalum spalls by percolation fracture mechanism due to rather large stress and strain linking ranges between voids and short loading times.

Acknowledgments: We are pleased to acknowledge the support from the Joint DoD/DOE Munitions Technology Development Program and the United States DOE. Carl Trujillo is thanked for performing the spall tests. Max Winkler is greatly appreciated for assistance and tutelage in setting up and operating the VISAR apparatus. Sheri Bingert annealed the samples. Mike Lopez assisted with the optical microscopy. Ron Ellis is thanked for illustrating assistance.

References

[1] A. K. Zurek, J. N. Johnson, and C. E. Frantz, *Journal de Physique*, *49*, C3, suppl. 9, (1988), 269.

[2] J. N. Johnson, *J. of Applied Physics*, *52*, 4, (1981), 2812.

[3] D. R. Curran, L. Seaman, and D. A. Shockey, *Physics Reports*, *147*, (1987), 253.

[4] L. M. Barker and R. E. Hollenbach, *J. Applied Physics*, *43*, 11, (1972), 4669.

[5] R. A. Graham and J. R. Asay, *High Temperature - High Pressure, 10*, (1978), 355.
[6] J. N. Johnson, R. S. Hixson, D. L. Tonks, *et al.*, in *Shock Compression of Condensed Matter*, edited by S. C. Schmidt and W. C. Tao (AIP, New York, 1996), in press.
[7] G. T. Gray, III, in *High-Pressure Science and Technology*, edited by S. C. Schmidt, J. W. Shaner, G. A. Samara and M. Ross (AIP, 1994).
[8] J. N. Johnson and P. S. Lomdahl, *J. de Physique, IV*, Collaque C3, (1991), 223.
[9] J. N. Johnson, P. S. Lomdahl, and J. M. Wills, *Acta Metallurgica, 39*, (1991), 3015.
[10] J. N. Johnson, R. S. Hixson, G. T. Gray, III, *et al.*, *J. of Applied Physics, 72*, (1992), 429.
[11] J. N. Johnson, in *High Pressure Shock Compression of Solids*, edited by J. R. Asay and M. Shahinpoor (Springer-Verlag, 1993), p. 217.
[12] J. N. Johnson, *J. of Physica and Chemistry of Solids, 54*, (1993), 691.
[13] J. N. Johnson, R. S. Hixson, D. L. Tonks, *et al.*, in *High Pressure Science and Technology-1993*, edited by S. C. Schmidt, J. W. Shaner, G. A. Samara and M. Ross (American Institute of Physics, 1993), Vol. 309, p. 1095.
[14] J. N. Johnson, in *High Pressure Science and Technology-1993*, edited by S. C. Schmidt, J. W. Shaner, G. A. Samara and M. Ross (American Institute of Physics, 1993), Vol. 309, p. 1145.
[15] G. T. Gray, III and A. D. Rollett, in *High Strain Rate Behavior of Refractory Metals and Alloys*, edited by R. Asfahani, E. Chen and A. Crowson (The Minerals, Metals and Materials Society, 1992), p. 303.
[16] R. W. Armstrong, J. H. Bechtold, and R. T. Begley, in *Refractory Metals and Alloys*, edited by R. Asfahani, E. Chen and A. Crowson (The Minerals, Metals and Materials Society, 1992).
[17] D. L. Tonks, A. K. Zurek, and W. R. Thissell, in *Metallurgical and Materials Applications of Shock-Wave and High-Strain-Rate Phenomena (EXPLOMET'95)*, edited by L. E. Murr, K. P. Staudhammer and M. A. Meyers (Elsevier, New York, 1995), p. 171.
[18] D. L. Tonks, *J. Physique, IV*, C8, 4, (1994), 665.
[19] D. L. Tonks, in *Dynamic Plasticity and Structural Behaviors*, edited by S. Tanimura and A. S. Khan (Gordon and Breach, Luxembourg, 1995), p. 119.
[20] D. L. Tonks, in *Shock Compression of Condensed Matter*, edited by L. Davison, D. E. Grady and M. Shahinpoor, 1995), Vol. IV, in press.
[21] D. L. Tonks, *work in progress*, (1996).